Biochem. J. (2010) **431**, 51–61 (Printed in Great Britain) doi:10.1042/BJ20100651

online data

Fragment-based screening by X-ray crystallography, MS and isothermal titration calorimetry to identify PNMT (phenylethanolamine N-methyltransferase) inhibitors

Nyssa DRINKWATER*, Hoan VU†, Kimberly M. LOVELL‡, Kevin R. CRISCIONE‡, Brett M. COLLINS*, Thomas E. PRISINZANO‡, Sally-Ann POULSEN†, Michael J. McLEISH§, Gary L. GRUNEWALD‡ and Jennifer L. MARTIN*[1]

*University of Queensland, Institute for Molecular Bioscience, Division of Chemistry and Structural Biology, Brisbane, Queensland 4072, Australia, †Griffith University, Eskitis Institute, Brisbane, Queensland 4111, Australia, ‡Department of Medicinal Chemistry, University of Kansas, Lawrence, KS 66045-7582, U.S.A., and §Department of Chemistry and Chemical Biology, Indiana University–Purdue University Indianapolis (IUPUI), 402 N. Blackford St, LD 326D, IN 46202, U.S.A.

CNS (central nervous system) adrenaline (epinephrine) is implicated in a wide range of physiological and pathological conditions. PNMT (phenylethanolamine N-methyltransferase) catalyses the final step in the biosynthesis of adrenaline, the conversion of noradrenaline (norepinephrine) to adrenaline by methylation. To help elucidate the role of CNS adrenaline, and to develop potential drug leads, potent, selective and CNS-active inhibitors are required. The fragment screening approach has advantages over other lead discovery methods including high hit rates, more efficient hits and the ability to sample chemical diversity more easily. In the present study we applied fragment-based screening approaches to the enzyme PNMT. We used crystallography as the primary screen and identified 12 hits from a small commercial library of 384 drug-like fragments. The hits include nine chemicals with two fused rings and three single-ring chemical systems. Eight of the hits come from three chemical classes: benzimidazoles (a known class of PNMT inhibitor), purines and quinolines. Nine of the hits have measurable binding affinities (~5–700 μM) as determined by isothermal titration calorimetry and all nine have ligand efficiencies of 0.39 kcal/mol per heavy atom or better (1 kcal ≈ 4.184 kJ). We synthesized five elaborated benzimidazole compounds and characterized their binding to PNMT, showing for the first time how this class of inhibitors interact with the noradrenaline-binding site. Finally, we performed a pilot study with PNMT for fragment-based screening by MS showing that this approach could be used as a fast and efficient first-pass screening method prior to characterization of binding mode and affinity of hits.

Key words: benzimidazole, catecholamine, drug discovery, enzyme inhibition, fragment-based screening, phenylethanolamine N-methyltransferase (PNMT).

INTRODUCTION

The identification of suitable starting compounds for development into drugs is a major challenge for drug discovery and development programmes. FBS (fragment-based screening) has been developed as a method for the rapid discovery and subsequent elaboration of hits into quality lead compounds [1,2]. This approach is based on the principle of screening simple low-molecular-mass compounds that make a few high-quality interactions with the target site. Resulting hits tend to bind to the targets efficiently yet with low affinity and, with a practically designed library, are readily tractable for follow up chemistry [3]. These fragment hits are used as 'anchors' that can be elaborated to fill additional regions of the target site. This results in potent compounds with minimal chemical complexity that can then be developed into drugs. A major challenge in establishing FBS has been the development of sensitive methods to detect the weak binding of hits (with typically milli- to micro-molar binding affinities) [4]. Methods currently used include ITC (isothermal titration calorimetry), NMR, surface plasmon resonance, MS and X-ray crystallography [1,5–7].

FBS-X (FBS by X-ray crystallography) provides the greatest level of information for the elaboration of hit compounds [8]. However, costly infrastructure for crystallization, crystal handling and data collection is required for screening hundreds of crystals in a high-throughput manner. Although many different FBS methods are now used, there have been few reports comparing hits identified against the same specific target by orthogonal methods. NMR is frequently employed as a first-pass screen before detailed structural characterization of hits by X-ray crystallography, and MS has the potential to be applied in a similar manner [9]. Comparative FBS-X and FBS-MS campaigns have not been reported, as far as we are aware, yet there are potentially significant advantages to a combined MS/X-ray screening approach due to their complementary attributes.

Pharmaceutical companies have developed and applied FBS-X with success [10]. An ideal target for FBS-X has an accessible active site, can be crystallized in the apo form and requires only minor conformational changes in the crystal form to accommodate ligand binding. However, many drug targets do not conform to these requirements, including the human enzyme PNMT (phenylethanolamine N-methyltransferase; EC

Abbreviations used: AdoHcy, *S*-adenosyl-L-homocysteine; AdoMet, *S*-adenosyl-L-methionine; CCD, charge-coupled-device; CNS, central nervous system; ESI, electrospray ionization, FBS, fragment-based screening, FBS-X, FBS by X-ray crystallography; FTMS, Fourier transform MS; HA, heavy atom; HRMS, high-resolution MS; ITC, isothermal titration calorimetry; LE, ligand-binding efficiency; m.p., melting point; MSD, Merck Sharp and Dohme Research Laboratories; PNMT, phenylethanolamine N-methyltransferase; hPNMT, human PNMT.

[1] To whom correspondence should be addressed (email j.martin@imb.uq.edu.au).

The co-ordinates and structure factors for all 17 crystal structures have been deposited with the PDB under accession codes 3KPJ, 3KPU, 3KPV, 3KPW, 3KPY, 3KQM, 3KQS, 3KQT, 3KQV, 3KQW, 3KQO, 3KQP, 3KQQ, 3KQY, 3KR0, 3KR1 and 3KR2.

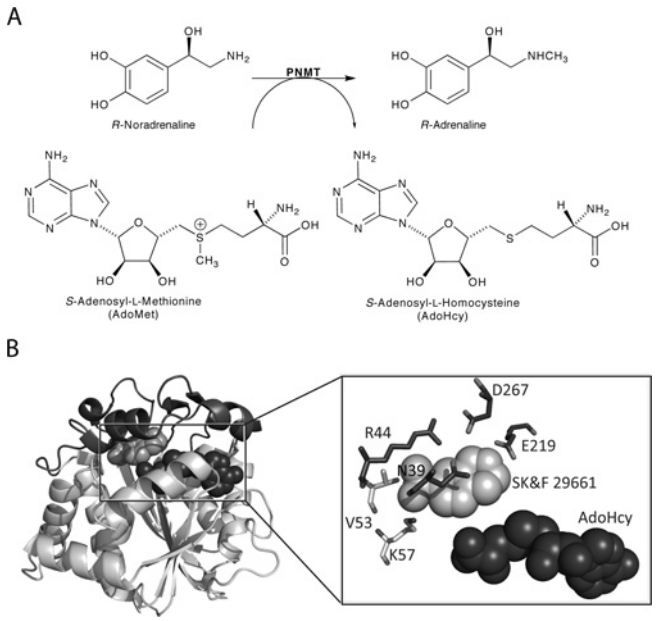

Figure 1 PNMT catalytic reaction

(**A**) The reaction catalysed by PNMT involves transfer of a methyl group from AdoMet to noradrenaline, forming adrenaline and AdoHcy. (**B**) The crystal structure of hPNMT–AdoHcy–SK&F29661, shown in dark grey and light grey space-filling representation respectively, are AdoHcy and SK&F29661; the Cα trace of hPNMT is shown predominantly in light grey, with the regions covering the AdoHcy- and SK&F29661-binding sites shown in dark grey. The boxed region shows a close-up of the AdoHcy- and SK&F29661-binding sites.

2.1.1.28; 30.7 kDa), which catalyses the final step in adrenaline (epinephrine) biosynthesis, the methylation of noradrenaline (norepinephrine) to form adrenaline (Figure 1A). PNMT has a potential role in a wide range of disease-relevant processes including the central control of blood pressure [11], pituitary hormone secretion [12], ethanol intoxication [13], Parkinson's disease [14] and the neurodegeneration observed in Alzheimer's disease [15]. Structures of recombinant hPNMT (human PNMT) in complex with inhibitors and substrates (e.g. PDB code 1HNN) show that hPNMT has an enclosed active site (Figure 1B) suggesting that enzyme conformational changes may be needed for ligands to bind [16]. Apo crystals are not readily available because we were unable to crystallize the enzyme in the absence of AdoHcy (*S*-adenosyl-L-homocysteine), which binds to the cofactor-binding site. Furthermore, when crystals are grown in the absence of an inhibitor or substrate at the noradrenaline-binding site, this site is occupied by a phosphate molecule [17]. However, we were encouraged to attempt FBS-X because we solved the crystal structure of hPNMT (PDB code 3HCD) in complex with the physiological substrate *R*-noradrenaline by using rapid soaking methods on hPNMT–AdoHcy–PO_4 crystals [17]. We therefore proposed to apply this same soaking method for FBS-X screening of hPNMT, with the aim of identifying novel chemical frameworks for inhibitor design. We also performed an FBS-MS pilot study to determine whether this approach could be used as a more efficient first-pass screen prior to crystallographic analysis of selected hits.

Overall, we showed that FBS-X can be successfully implemented within an academic environment. Our crystallographic screening of the non-ideal enzyme target hPNMT identified 12 hits, including three benzimidazoles (a known class of PNMT inhibitors), and nine of the hits could be characterized by ITC. Five compounds were synthesized to further characterize the benzimidazole class. Our pilot study showed that the orthogonal screening method of FBS-MS could be used as an even more efficient first step in an FBS campaign.

EXPERIMENTAL

Materials

The FBS library was purchased from ActiveSight (a Rigaku company), and comprised 384 compounds with a mean molecular mass of 142 Da and of predominantly rigid low-complexity (see the Supplementary Table Library at http://www.BiochemJ.org/bj/431/bj4310051add.htm); all compounds were provided as 200 mM stock solutions in 100 % DMSO and as cocktails of four fragments each at 50 mM in 100 % DMSO. All the compounds are also available for purchase directly from Sigma–Aldrich. For chemical syntheses, all reagents and solvents used were reagent grade and of the highest purity commercially available. 4-Methoxybenzene-1,2-diamine was sourced from Alfa Aesar, all other compounds and reagents were sourced from Sigma–Aldrich.

Crystallization of hPNMT

C-terminally His_6-tagged hPNMT was expressed and purified as described previously [18]. The protein was concentrated to 50 mg/ml and mixed with AdoHcy (to a final concentration of 2 mM) taking the final concentration of protein to 40 mg/ml or 1.25 mM. The protein mixture was crystallized by hanging drop vapour diffusion using QIAGEN EasyXtal Tool crystallization trays for ease of soaking. Drops comprised 1.5 μl of protein and 1.5 μl of precipitant equilibrated over 400 μl of precipitant solution {4–8 % PEG [poly(ethylene glycol)] 6000, 0.25 M LiCl and 0.1 M sodium cacodylate, pH 5.5–6.0}.

FBS by X-ray crystallography

Library screening was conducted blind, in that we made no assumptions about the contents of the library, or what compounds might be expected to bind PNMT. Prior to screening, control experiments were performed using known hPNMT inhibitors to confirm that ligands could be soaked into hPNMT–AdoHcy–PO_4 crystals and that the solvents used for fragment screening and cryoprotection did not interfere with binding. Crystals ($\sim$0.25 mm in each dimension) were transferred into 1 μl of soaking solution. Crystal soak solutions were prepared by adding 1 μl of fragment cocktail to 9 μl of stabilizing solution, taking the final concentrations to 6.6 % PEG 6000, 0.3 M LiCl, 0.1 M sodium cacodylate, pH 5.7, 4 $\times$ 5 mM fragments and 10 % (v/v) DMSO. Crystals were soaked for 15 min.

Crystals were cryoprotected by transferring directly from the soak solution into mother liquor supplemented with 25 % ethylene glycol for 10–15 s before being flash-cooled. Data for hPNMT–AdoHcy–PO_4 were measured from a crystal transferred directly into the cryoprotectant solution without undergoing a soak step. X-ray diffraction data from hPNMT crystals were measured using the UQ ROCX Diffraction Facility or the Australian Synchrotron. At the UQ ROCX Diffraction Facility, crystals were irradiated with X-rays of wavelength 1.542 Å (1 Å = 0.1 nm) generated from a Rigaku FR-E Superbright copper rotating anode generator operating at 45 kV, 45 mA and data were measured using one of two alternate methods: (i) crystals were flash-cooled by plunging into liquid nitrogen and placed on the camera using a Rigaku ACTOR™ crystal mounting robot, X-rays were focused with Osmic Vari-Max HF optics and diffraction data

measured on a Rigaku Saturn 944 CCD (charge-coupled-device) detector; or (ii) crystals were flash-cooled on the camera in the gaseous nitrogen stream at 100K, X-rays were focused with Osmic HiRes^2 Confocal Max-Flux™ optics and diffraction data measured with a Rigaku R-AXIS IV^{++} imaging plate area detector. Data collected at UQ ROCX Diffraction Facility were processed using Crystal Clear (Rigaku). Data collected at the Australian Synchrotron were measured at 100K with X-rays of wavelength 0.95667 Å on beamline 3BM1 [19] using a MAR 165 CCD detector, and processed using HKL2000 [20]. Crystals diffracting to better than 2.7 Å resolution were used for data collection.

Phasing and automatic structure solution were carried out using MIfit (ActiveSight). The structures were solved by molecular replacement using the structure of hPNMT–AdoHcy–SK&F29661 (PDB code 1HNN), with the inhibitor and waters removed, as the starting model. Active-site density was individually evaluated and assessed for the presence or absence of a ligand. If density indicating a bound fragment was present, ligands were modelled manually using COOT [21] and co-ordinates and refinement parameters were generated by PRODRG [22] and PHENIX [23]. Further refinement was carried out using PHENIX [23]. Cross-validation was done by *R*-free analysis from 5 % of the reflections set aside from refinement.

Where density was present at the active site but did not unambiguously identify the bound ligand from the four compounds in the cocktail, a deconvolution step was performed. This involved collecting data from crystals soaked in solutions containing the individual compounds (rather than the cocktail of four compounds). In these cases, the final concentration of the compounds in the soak solution was increased to 20 mM rather than the 5 mM concentration used in the cocktail screen. The higher concentration generally resulted in improved density. Deconvolution also allowed identification of the binding of more than one fragment per cocktail.

Structure determination of hPNMT in complex with elaborated benzimidazoles

Compounds 13–17 were designed and synthesized (see below for details of synthesis) to further characterize the binding of benzimidazoles to hPNMT. The crystal structures of these compounds in complex with hPNMT were determined as follows. Crystals of hPNMT–AdoHcy–PO_4 were soaked in a solution of the synthesized compounds as described above for fragment screening. In this case, compounds were solubilized at 100 mM in 50 % DMSO/water and used to prepare soak solutions of final concentrations 6.6 % PEG 6000, 0.3 M LiCl, 0.1 M sodium cacodylate, pH 5.7, 5–10 mM compounds and 2.5–5 % DMSO.

Crystals were cryoprotected, diffraction data collected and processed, and structures solved and refined at the UQ ROCX diffraction facility using method (ii) described above, with the exception that phasing was carried out using PHENIX [23] and structures were solved by difference Fourier methods. The procedure in this case was to model and refine the structure of the protein first, followed by addition of water molecules, then AdoHcy and finally the ligand. The criteria used to include a water molecule were: the presence of $2F_o-F_c$ density at 1σ and F_o-F_c density at 3σ and at least one possible hydrogen bond within 3.2 Å. Cross-validation was performed as described above. All of the crystal structure electron density maps revealed density indicative of AdoHcy at the cofactor-binding site and density consistent with a benzimidazole bound at the noradrenaline-binding site.

FBS by MS

MS was performed on an APEX® III 4.7 Tesla FTICR mass spectrometer (Bruker Daltonics) fitted with an Apollo™ ESI (electrospray ionization) source operated in positive ion mode. XMASS NT V6.1.2 MS software on a PC platform was used for data acquisition. Broadband excitation was used to analyse a mass range from m/z 50–6000 and each spectrum was an average of 64 transients (scans) with 512 000 data points acquired in low-resolution mode with an acquisition time of approx. 4 min/sample. Samples were infused into the ESI source at 2 μl/min. Nitrogen was used as both the drying gas (125 °C) and nebulizing gas. Relevant parameters include a 10^4-fold pressure reduction between source and analyser regions with an ESI source pressure (10^{-7} kPa) and high-vacuum analyser region pressure (6×10^{-11} kPa). Agilent ESI tuning mix (Santa Clara) was used for an external three-point calibration. The hexapole ion accumulation time was 3 s.

To confirm correct ESI-MS parameter adjustment, parameters were optimized using a known hPNMT ligand (7-aminosulfonyl-3-ethyl-1,2,3,4-tetrahydroisoquinoline; K_i of 1.8 μM) [24]. Fragments analysed (Supplementary Figure S1 at http://www.BiochemJ.org/bj/431/bj4310051add.htm) were selected to include a range of FBS-X-positive and -negative hits. A total of 12 fragments were provided with no indication as to which compounds were hits by FBS-X. A stock solution of 31.5 μM hPNMT was prepared in 10 mM ammonium acetate (pH 7); stock solutions of AdoHcy and each of the 12 fragments (representing three of the FBS-X cocktails) were prepared in methanol. Aliquots of all solutions were used immediately or stored at −30 °C. Samples for MS analysis were prepared as follows: 3 μM hPNMT, 0 or 30 μM AdoHcy and 300 μM (100 equiv.) fragment in a total volume of 100 μl. Samples were incubated at room temperature (25 °C) for 30 min prior to MS analysis. A total of 24 MS datasets were acquired to analyse the 12 fragments (i.e. with and without added AdoHcy cofactor). The protein consumption per 100 μl sample was 0.01 mg, however, this sample volume was prepared for convenience and could be reduced as the consumed sample volume was 8 μl per MS acquisition (4 min acquisition at 2 μl/min).

If a hPNMT–fragment or hPNMT–AdoHcy– fragment non-covalent complex is formed in solution then the complex was observed in the ESI mass spectrum. The mass difference between the peaks for the unbound hPNMT and the hPNMT–fragment ($\Delta m/z$) can be multiplied by the charge state to give directly the molecular mass of the binding fragment i.e. M_r fragment $= \Delta m/z \times z$ to provide confirmation of the identity of the hit fragment. Complexes with AdoHcy were similarly treated to identify and confirm the fragment hits. ESI-FT (Fourier transform) MS analysis of a solution containing 3 μM hPNMT yielded the ESI positive ion mass spectrum shown in Supplementary Figure S2(A) at http://www.BiochemJ.org/bj/431/bj4310051add.htm. Peaks corresponding to the 13^+ to 10^+ charge states of hPNMT were observed. The ESI-FTMS spectrum of 3 μM hPNMT with added 30 μM AdoHcy yielded the ESI positive ion mass spectrum shown in Supplementary Figure S2(B) and, as an example, the ESI-FTMS mass spectrum of a hPNMT–AdoHcy–hit (compound 6) solution is shown in Supplementary Figure S2(C). In this spectrum each charge state consists of a peak corresponding to hPNMT–AdoHcy and a peak corresponding to the hPNMT–AdoHcy–fragment non-covalent complex. Actual mass values of the peaks observed in Supplementary Figure S2(C) and calculation of the mass of the fragment hit with compound 6 are given in Supplementary Table S1 at http://www.BiochemJ.org/bj/431/bj4310051add.htm.

ITC

Compounds found to bind hPNMT by FBS-X or FBS-MS were subsequently analysed by ITC. ITC was carried out using a high-sensitivity MicroCal (GE Healthcare) iTC_{200} system at 25 °C. Purified protein at a concentration of 200 μM plus 600 μM AdoMet (*S*-adenosyl-L-methionine) in 20 mM Tris/HCl, pH 7.2, 1 mM EDTA and 4.3 % DMSO were loaded into the sample cell (V_{cell}, reaction cell volume of $\approx$200 μl). DMSO in the sample was calibrated to match the residual DMSO after fragment dilutions. The fragment hit at 1.5–3 mM in the same buffer was then titrated into the sample cell with 20 × 2.5 μl injections. The heat released was measured and integrated using MicroCal Origin 7.0 software. The association constant (K_a; $1/K_d$), enthalpy (ΔH) and stoichiometry (N) were calculated using a single-site binding model. Measurements were repeated 2–4 times for each ligand and errors calculated as the S.D. from replicate experiments. In each case the protein concentration was fixed as a known quantity and the apparent ligand concentration was adjusted slightly during curve fitting so that the binding stoichiometry was approx. 1 (i.e. an assumption of 1:1 binding was made).

The energies of interaction were calculated from K_a values using the Gibbs free energy equation: $\Delta G = -RT(\ln K_a)$, where R is the gas constant (1.9872 kcal/mol; 1 kcal $\approx$ 4.184 kJ), T is the temperature of the experiment (298 K) and K_a is the association constant for the compound. LE (ligand-binding efficiency) values were calculated according to $LE = -\Delta G/HA$, where ΔG is the free energy of binding (kcal/mol) and HA is the number of heavy atoms (non-hydrogen atoms) in the compound.

Compound synthesis

Benzimidazoles (compounds 13–17, see Figure 5) were synthesized using procedures published previously with minor modifications as indicated (see the Supplementary Experimental section at http://www.BiochemJ.org/bj/431/bj4310051add.htm). Generally, an appropriately substituted nitroaniline was reduced by palladium-catalysed hydrogenation to the corresponding phenylenediamine. The phenylenediamine derivative was condensed with cyanogen bromide to form the desired 2-aminobenzimidazole as the hydrobromide salt. Methoxy-substituted 2-aminobenzimidazoles were converted to their corresponding phenol derivatives using 48 % hydrogen bromide. Compounds 13 and 17 have not been reported previously and details of their synthesis are reported below. Compounds 14–16 are known compounds and the details of our syntheses of them are given in the Supplementary Experimental section.

The m.p. (melting point) was determined in open capillary tubes on a Thomas–Hoover melting point apparatus calibrated with known compounds, but are uncorrected. Proton (^{1}H-NMR) and carbon (^{13}C-NMR) NMR spectra were taken on a Bruker DRX-500 spectrophotometer. Proton chemical shifts are reported in p.p.m. relative to TMS (tetramethylsilane; 0.00 p.p.m.) or to methanol-d_4 (3.31 p.p.m.). Carbon chemical shifts are reported in p.p.m. relative to C^2HCl_3 (77.2 p.p.m.) or methanol-d_4 (49.1 p.p.m.). HRMS (high-resolution MS) was performed on a Ribermag R 10-10 mass spectrophotometer. Hexane refers to the mixture of hexane isomers (boiling point of 68–70 °C).

2-Amino-4(7)-hydroxybenzimidazole · hydrobromide (compound 13 · HBr)

Ether-mediated cleavage [25] of 2-amino-4(7)-methoxybenzimidazole [25] (compound 18) was performed by dissolving compound 18 (0.40 g, 2.4 mmol) in 20 ml of 48 % hydrogen bromide. The solution was refluxed at 100 °C for 16 h. The reaction was washed with diethyl ether and evaporated under reduced pressure to yield the crude compound 13 · HBr as a brown solid. Trituration from 2-propanol/hexane yielded a viscous brown liquid that was dried *in vacuo* to yield 13 · HBr as a brown solid (0.24 g, 66 %), m.p. >250 °C: ^{1}H-NMR (500 MHz, MeOD) δ 7.07 (t, $J = 8.1$, 1H), 6.84 (d, $J = 7.5$, 1H), 6.70 (dd, $J = 0.6$, 8.1, 1H); ^{13}C-NMR (126 MHz, MeOD) δ 151.8, 145.0, 132.7, 125.9, 119.7, 110.8, 103.6; HRMS (*m/z*): [M+H] calculated for $C_7H_7N_3OBr$, 227.9772, found 227.9775.

2-Amino-5(6)-chloro-7(4)-hydroxybenzimidazole · hydrobromide (compound 17 · HBr)

Reduction [26] of 4-chloro-2-methoxy-6-nitroaniline [27] (compound 19) was performed by dissolving compound 19 (0.30 g, 1.8 mmol) in methanol (40 ml) and adding 30 mg of 10 % palladium on carbon. The mixture was stirred under hydrogen for 16 h. The palladium was removed by filtration over Celite®. The Celite® was washed with methanol and ethyl acetate. The combined organic washes were concentrated under reduced pressure to a viscous brown liquid. Column chromatography (silica gel, ethyl acetate/hexanes of 3:7) yielded 5-chloro-3-methoxybenzene-1,2-diamine (compound 20) as a brown solid (0.18 g, 58 %) that was used for the next synthetic step without further purification: m.p., 97–99 °C; ^{1}H-NMR (500 MHz, $CDCl_3$) δ 6.39 (dd, $J = 2.1$, 4.4, 2H), 3.82 (s, 3H), 3.42 (s, 4H); ^{13}C-NMR (126 MHz, C^2HCl_3) δ 149.0, 136.4, 124.5, 122.0, 109.7, 103.3, 56.1; HRMS (*m/z*): [M+H] calculated for $C_7H_{10}ClN_2O$, 173.0482; found 173.0373.

Diamine compound 20 (0.18 g, 1.0 mmol) was dissolved in acetonitrile (20 ml) and water (5 ml) and cooled to 0 °C. Cyanogen bromide in acetonitrile (5M, 0.20 ml, 1.0 mmol) was added dropwise over 5 min. The reaction mixture was warmed to room temperature and stirred overnight. The solvents were evaporated under reduced pressure to give 2-amino-5(6)-chloro-7(4)-methoxybenzimidazole · hydrobromide (compound 21 · HBr) as a brown solid (0.30 g), which was used for the next synthetic step without further purification, m.p., 68–70 °C: ^{1}H-NMR (500 MHz, MeOD) δ 7.01 (d, $J = 1.6$, 1H), 6.94 (d, $J = 1.6$, 1H), 3.98 (s, 3H); ^{13}C-NMR (126 MHz, MeOD) δ 152.6, 147.5, 132.8, 131.2, 119.4, 107.9, 105.6, 57.1; HRMS (*m/z*): [M+H] calculated for $C_8H_9ClN_3O$, 198.0434; found 198.0383.

Ether cleavage of compound 21 · HBr was carried out using the procedure given for the synthesis of compound 13 · HBr above, yielding compound 17 · HBr as a brown solid (0.10 g, 36 %), m.p. >250 °C: ^{1}H-NMR (500 MHz, MeOD) δ 6.88 (d, $J = 1.7$, 1H), 6.72 (d, $J = 1.7$, 1H); ^{13}C-NMR (126 MHz, MeOD) δ 152.3, 145.5, 133.1, 130.7, 118.8, 111.2, 104.0; HRMS (*m/z*): [M+H] calculated for $C_7H_7N_3OCl$, 184.0278; found 184.0266.

RESULTS

FBS-X

For the FBS-X experiments, we used crystals of hPNMT grown in the absence of inhibitor or ligand for the noradrenaline-binding site. The crystal structure resulting from such crystals reveals a phosphate molecule bound in the noradrenaline-binding site (Figure 2); the phosphate apparently co-purifies with the enzyme during an affinity purification step. The phosphate forms favourable interactions with the side chains of Lys^{57} and Asn^{39}. For a hit to be detected in the FBS-X experiments, one or more of the four fragments of the cocktail must displace the

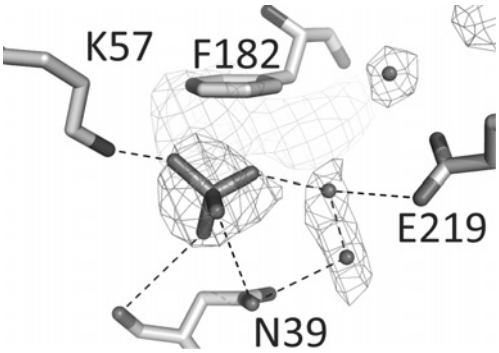

Figure 2 hPNMT noradrenaline-binding site

The hPNMT target binding site for inhibitors is shown for the enzyme crystallized in the absence of inhibitor/substrate. This crystal form was used for FBS-X screening. The phosphate molecule in the noradrenaline site must be displaced by a soaked fragment for a hit to be detected.

Table 1 Statistics for FBS-X screening on hPNMT

The hit rate is calculated on the basis of 12 hits from 376 screened compounds.

Parameter	Results
Number of compounds in library/number screened	384/376
Number of datasets collected in first round screen	94
Number of datasets collected in deconvolution steps	51
Average dataset resolution	2.5 Å
Average R_{work}/R_{free}	0.232/0.298
Number of hits	12
Hit rate	3.2%
Average resolution of hit structures	2.4 Å
Average R_{work}/R_{free} of hit structures	0.255/0.281

phosphate during the 15 min soaking step. Data collection and refinement statistics for a representative crystal structure of hPNMT–AdoHcy–PO_4 are included in Supplementary Table S2 at http://www.BiochemJ.org/bj/431/bj4310051add.htm.

Of the 96 cocktails containing four compounds (384 compounds in total) in the library, X-ray diffraction data were collected for 94 cocktails (Table 1). Two of the 96 cocktails caused crystal cracking during the soak, preventing high-resolution diffraction data measurement. Owing to the high-throughput nature of the screen, these two cocktails were not considered further. Evaluation of the eight compounds in these two cocktails will be investigated in another study. A total of 16 of the 94 cocktail soaks gave electron density suggestive of hits, i.e. binding of a chemical to the noradrenaline-binding site. The chemical identity of two of the hits was obvious from the initial X-ray data. An additional 51 datasets were measured to deconvolute hits where it was not clear which compound of the cocktail had bound or to measure higher resolution data for confirmed hits. During this process, four of the initially identified hits were found to be false positives. In summary, a total of 12 compounds (out of a possible 376) were identified as binding in the target site of hPNMT, giving a hit rate of 3.2 % for the FBS-X process. The $2F_o-F_c$ maps showing the ligand density for these 12 hits are provided as Supplementary Figure S3 at http://www.BiochemJ.org/bj/431/bj4310051add.htm. Summary statistics for the X-ray data are given in Table 1 and data collection and refinement statistics for the 12 hit crystal structures are included as Supplementary Table S2. The structures of the 12 hits and their binding mode to hPNMT are shown in Figure 3.

Analysis of fragment hits

The 12 fragment hits all bind the noradrenaline-binding pocket of hPNMT, the same site as other structurally characterized hPNMT inhibitors. Furthermore, all 12 fragments bind within the same region of the pocket (Figure 4A). All 12 fragment hits contain either or both a five- or six-membered aromatic ring, sandwiched between the side chains of Phe^{182} and Asn^{39}. In this position, the rings form $\pi-\pi$ stacking interactions with the side chain of Phe^{182}. The importance of this interaction is evident in the structure of 6-chloro-oxindole (compound 4) bound to hPNMT (Figure 3). Unlike other ligand-bound hPNMT structures, there are no direct hydrogen-bond interactions formed between compound 4 and hPNMT. In addition to the $\pi-\pi$ stacking interactions between the benzene ring and Phe^{182}, the only other interaction that might contribute to binding of compound 4 is a hydrophobic interaction between the chlorine atom and the aromatic ring of Tyr^{222}.

Three chemical frameworks are present in more than one fragment hit: (i) the benzimidazole core (compounds 6, 7, and 9); (ii) the purine core (compounds 2 and 10); and (iii) the quinoline core (compounds 1, 3 and 11). Despite different substituents, the benzimidazole-based fragments all bind in the same orientation within the active site. In contrast, the binding modes of the two purine-based fragments and the three quinoline fragments vary. This variation allows different functional groups to make favourable interactions (e.g. see compounds 2 and 10, in Figure 3) demonstrating that the presence of substituents can alter the binding pose of a core fragment. It should also be noted that the library used for FBS-X screening contains a further ten benzimidazole compounds, none of which were found to bind the noradrenaline site. Similarly, the screening library also contained other quinolines and purines that did not bind to the target site under the conditions used for FBS-X. The observation that different substituents affect binding of compounds to PNMT provides further validation for the specificity of hits identified by FBS-X and may be useful for structure–activity relationship analysis in the development of more potent inhibitors.

Superposition of the fragment hits demonstrates how opposite ends of the noradrenaline pocket bind different chemical functionalities (Figures 4A and 4B). Hydrophilic nitrogen and oxygen atoms of hit compounds are clustered at one end of the pocket, forming direct and water-mediated interactions with the active-site residues Glu^{185}, Glu^{219}, Asp^{267} and the main chain of Phe^{182}. In contrast, carbon and chlorine atoms of hit compounds are clustered at a hydrophobic region of the pocket consisting of the side chains of Val^{53}, Met^{258}, Val^{269} and Val^{272}. These same amino acid residues are involved in binding characterized previously between inhibitors and substrates [28–30].

In some cases, we found unfavourable contacts between the fragments and hPNMT residues. Many unfavourable interactions resulted from clashes with the hydroxy group of Tyr^{35}, which is close to the hydrophobic residues Val^{53}, Met^{258}, Val^{269} and Val^{272}. We also observed cases where the electron density for all or part of the fragment was weak. For example, density for the flexible chain of formanilide (compound 8) is weak. In two other cases, 1-aminoisoquinoline (compound 3) and 2-hydroxynicotinic acid (compound 12), the fragments adopt different binding poses in the two hPNMT molecules in the asymmetric unit. This may be due to a lower affinity of these ligands compared with other hits. Finally, for 4-bromo-1*H*-imidazole (compound 5), it was difficult to determine from the electron density alone the correct position

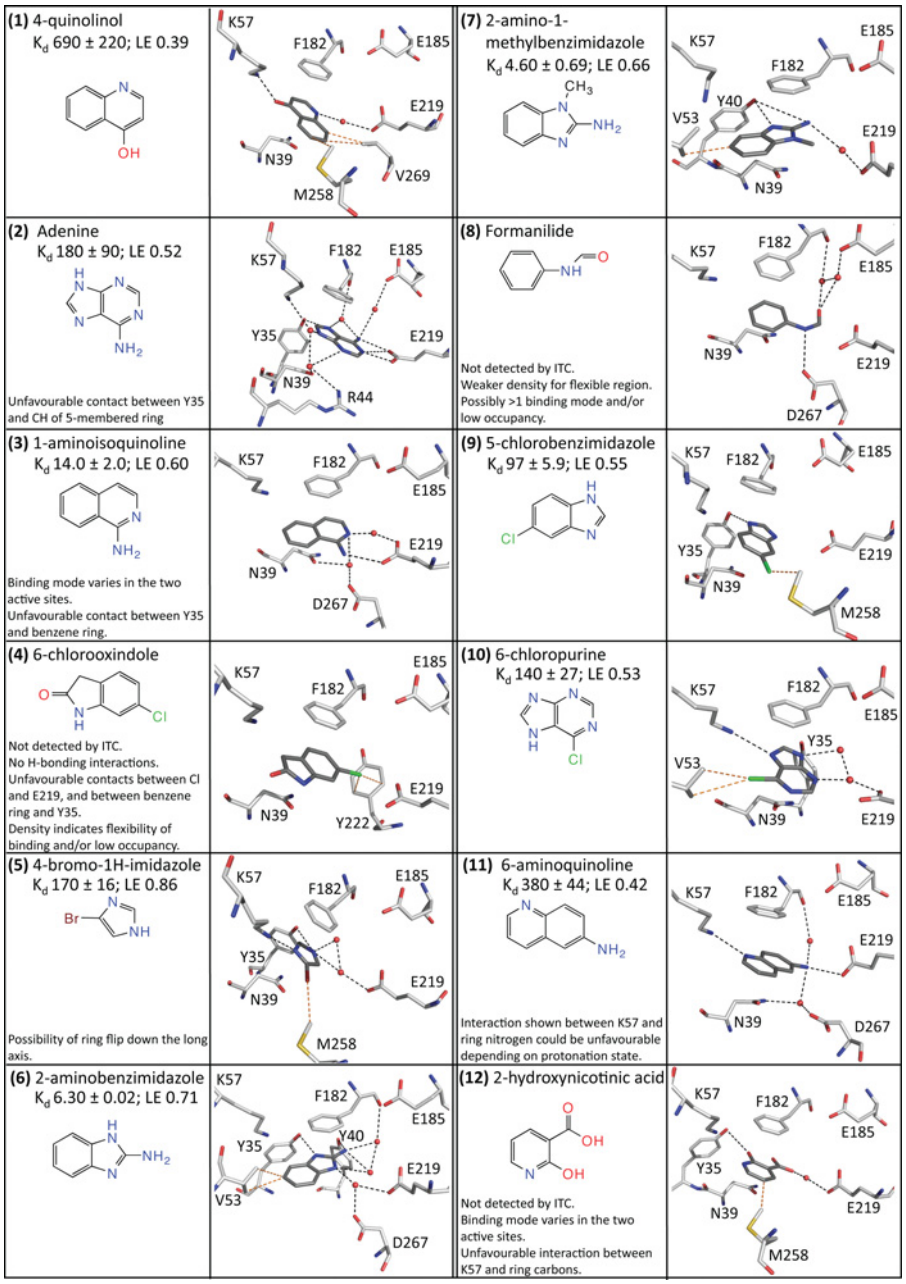

Figure 3 Summary of the results of FBS-X targeting hPNMT

The 12 fragment hits were identified, and the chemical structures and binding poses of each are shown. Hydrogen bond interactions are shown as black and hydrophobic interactions are shown as orange broken lines. Binding affinities determined by ITC (K_d in μM $\pm$ S.D.) and calculated LE values (in kcal/mol per HA) are given for each hit.

of the ring nitrogen atoms because the compound fits the density equally well in two orientations, rotated 180° around the long axis. Compound 5 was modelled in one orientation on the basis of predicted favourable interactions (see Figure 3).

Water molecules in the active site are important because they can indicate potential areas for favourable elaboration of fragments. We found that many water molecules are conserved across the 12 enzyme–fragment structures (Figure 4C). There are five major water-binding sites, four of which are located in the hydrophilic region of the binding pocket described above. These four sites, show the greatest level of conservation across the 12 structures, and mediate interactions with Glu^{185}, Glu^{219} and Asp^{267}. The presence of defined water-binding pockets suggests that these regions favour ligand interactions and would probably be amenable to interactions with elaborated inhibitors.

FBS by MS

MS has high sensitivity and a wide dynamic range and can be used to detect non-covalent complexes with a K_d in the range from 10 nM to 1 mM [9]. We were interested in using MS as a first-pass FBS method, so we performed a pilot study on hPNMT to ascertain whether MS could identify the same hits as FBS-X. For proof-of-concept, an ESI-FTMS analysis was conducted on a subset of 12 of the 384 fragments from the library.

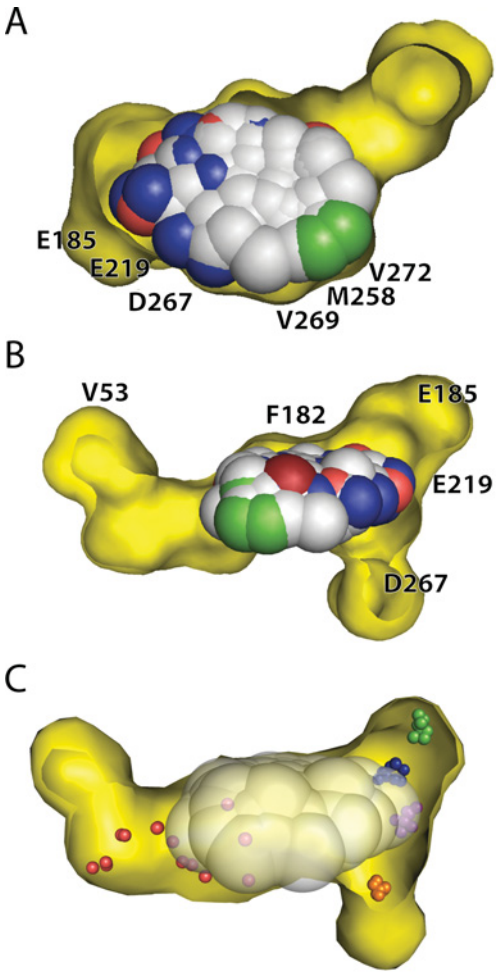

Figure 4 Solvent accessible surface of the hPNMT active site showing the overlaid structures of the 12 FBS-X hits

(**A** and **B**) Binding positions of the FBS-X hits in the hPNMT target site, shown in two different orientations. The 12 fragment hits are shown superimposed in space-filling representation (oxygen atoms in red, nitrogen atoms in blue, carbon atoms in white and chlorine atoms in green). The positions of residues discussed in the text are indicated, although for clarity the structures of these residues are not shown. (**C**) Water molecules are bound in five major sub-sites represented by green, blue, purple, orange or red spheres. Fragment hits are shown in transparent space filling representation. This panel is shown in the same orientation as (**B**).

The 12 fragments were intentionally chosen to include several FBS-X hits. ESI-FTMS screening was conducted blind in that the researcher collecting and analysing the data did not know which of the 12 compounds were FBS-X hits. Of the 12 fragments tested, FBS-X identified four fragments as hits (compounds 1, 6, 11 and 12; Figure 3), three of which were detected by ESI-FTMS on first inspection of the data (compounds 1, 6 and 12). The fourth FBS-X hit, compound 11, was detected upon re-evaluation of the ESI-FTMS spectra, although it was identified as a weak complex. In addition, ESI-FTMS identified two other hits (Supplementary Figure S3); these two fragments were not identified by FBS-X.

ITC evaluation of fragment hits

To confirm and characterize further the 14 fragment hits (12 identified by FBS-X and the two identified by ESI-FTMS), and to prioritize the fragment hits for follow up chemistry and optimization, ITC was used to determine their dissociation constants (K_d) for hPNMT, and thermodynamic parameters of binding. All of the nine fragment hits detected by ITC demonstrated favourable enthalpic contributions (Figure 3 and Table 2). Of the 12 FBS-X hits, the measured binding affinities for nine fragments ranged from approx. 5 to 700 μM. Of these, two fragments (compounds 1 and 11) show low-affinity binding (below 200 μM) that results in sub-optimal Wiseman *c*-values (<1) for accurate affinity determination by ITC and this is reflected in the relatively large errors [31]. Nonetheless the data do allow prioritization of these compounds for follow-up. Binding of the remaining three FBS-X hits (compounds 4, 8 and 12) could not be detected by ITC. The two additional hits identified by ESI-FTMS were also not detected by ITC. Furthermore, whereas the binding of 4-quinolinol (compound 1) was detected in ITC experiments, and a K_d of 0.7 mM was calculated from the ITC measurements, the signal was weak. The two tightest binding fragments with K_d values of approx. 5 μM (2-aminobenzimidazole, compound 6, and 2-amino-1-methybenzimidazole, compound 7), are both based on the benzimidazole core. As discussed above, benzimidazoles have been shown previously to inhibit PNMT [32]. The third fragment hit with a benzimidazole core (5-chlorobenzimidazole, compound 9), had a 20-fold lower binding affinity (K_d of 97 μM), suggesting that direct and water-mediated hydrogen bonds to the 2-amino groups of compounds 6 and 7 contribute considerably to ligand affinity for hPNMT. The dissociation constants were used to calculate their LE values (Figure 3 and Table 2). The LE values ranged from 0.39 kcal/mol per HA for 4-quinolinol to 0.86 kcal/mol per HA for 4-bromo-1*H*-imidazole (compound 5). The two tightest binding benzimidazole-based fragments, compounds 6 and 7, had high LEs of $\sim$0.7 kcal/mol per HA.

Elaborated benzimidazole compounds

Three of the identified hits (compounds 6, 7 and 9) contain a benzimidazole ring system. The electron density for these three hits was excellent, and ITC measurements confirmed that all three bind to hPNMT, two of them with very high LE values. Benzimidazoles have been investigated previously as inhibitors of PNMT, although the earlier work was performed on the bovine enzyme [32]. To further characterize the interaction of benzimidazole-based fragments with the human enzyme, a series of compounds (compounds 13–17; Figure 5) closely related to the FBS-X benzimidazole hits were synthesized. The 2-amino group was retained in this series because in compounds 6 and 7 it forms direct and water-mediated hydrogen bonds to the enzyme. The binding of compounds 13–17 to hPNMT was evaluated by ITC and X-ray crystallography. The results of these analyses are shown in Figure 5 and data collection and refinement statistics for the structures are included as Supplementary Table S2. ITC curves are shown in Supplementary Figure S4 at http://www.BiochemJ.org/bj/431/bj4310051add.htm, and the ITC-derived thermodynamic parameters of the 12 fragment hits and five elaborated compounds are given in Table 2.

Hydroxy-substituted 2-aminobenzimidazole compounds (compounds 13 and 14)

Superposition of the benzimidazole-based fragments with the fragment hit 4-quinolinol (compound 1), suggested that a hydroxy group added to the 7- or 6- position of compound 6 would interact with Lys[57] and potentially with Tyr[40]. To test this, compounds 13 and 14 were synthesized and their binding characterized (Figure 5 and Table 2). The crystal structures of

Table 2 Thermodynamic parameters determined by ITC

Errors are S.D., calculated from averaging results for the replicates.

Compound	Number of replicates used	Stoichiometry (N)	Wiseman *c*-value	ΔG (kcal/mol)	ΔH (kcal/mol)	$-T\Delta S$ (kcal/mol)	K_d (μM)	LE (kcal/mol per HA)
1	2	0.8	0.3	−4.34 ± 0.28	−11.12 ± 4.76	6.78 ± 5.0	690 ± 220	0.39
2	2	1.3	1.1	−5.20 ± 0.47	−9.03 ± 5.74	3.83 ± 6.21	180 ± 90	0.52
3	4	0.9	14.3	−6.63 ± 0.09	−11.60 ± 1.13	4.97 ± 1.22	14.0 ± 2.0	0.60
4	–	–	–	–	–	–	–	–
5	2	1.0	1.2	−5.15 ± 0.09	−10.19 ± 1.52	5.04 ± 1.43	170 ± 16	0.86
6	3	1.0	31.7	−7.10 ± 0.01	−12.37 ± 0.73	5.26 ± 0.72	6.30 ± 0.02	0.71
7	2	1.0	43.5	−7.30 ± 0.14	−11.73 ± 1.59	4.43 ± 1.45	4.60 ± 0.69	0.66
8	–	–	–	–	–	–	–	–
9	2	1.2	2.1	−5.47 ± 0.06	−8.56 ± 2.15	3.09 ± 2.21	97 ± 5.9	0.55
10	2	0.9	1.4	−5.25 ± 0.17	−11.54 ± 3.62	6.29 ± 3.79	140 ± 27	0.53
11	2	0.9	0.5	−4.66 ± 0.10	−8.69 ± 1.33	4.02 ± 1.43	380 ± 44	0.42
12	–	–	–	–	–	–	–	–
13	3	1.0	13.3	−6.58 ± 0.05	−7.20 ± 0.54	0.62 ± 0.52	15 ± 1.0	0.60
14	3	0.9	10.0	−6.40 ± 0.09	−7.57 ± 0.23	1.16 ± 0.15	20 ± 2.5	0.58
15	3	1.0	111	−7.96 ± 0.01	−11.70 ± 1.60	−3.73 ± 1.52	1.8 ± 0.3	0.72
16	3	1.0	27	−6.99 ± 0.01	−7.35 ± 0.65	−0.36 ± 0.70	7.2 ± 0.9	0.64
17	3	0.9	14.3	−6.62 ± 0.04	−10.13 ± 1.25	3.51 ± 1.27	14 ± 0.8	0.55

hPNMT–AdoHcy–compound 13 and hPNMT–AdoHcy–compound 14 showed that both these elaborated compounds bound in a flipped binding mode compared with the predicted binding mode, i.e. instead of forming an interaction with Lys[57], the hydroxy group is oriented away from Lys[57]. In hPNMT–AdoHcy–compound 13 the hydroxy group makes no favourable interactions, and sits in a hydrophobic pocket comprising the side chains of Met[258] and Val[269]. This same position is occupied by the chloro substituent of compound 9 when it forms a complex with hPNMT (Figure 3). In addition, the benzimidazole core of compound 13 is shifted away from the hydrophobic pocket compared with the original hit fragment, compound 6. This movement results in an unfavourable interaction between the six-membered aromatic ring and Lys[57]. These changes result in a reduced enthalpic binding contribution of compound 13 compared with compound 6; this is balanced by a smaller entropy loss upon binding with overall a small net decrease in the free energy of binding. This is reflected in a decreased binding affinity and LE of the elaborated compound compared with the original hit (compound 13, K_d of 15 μM and LE of 0.60 kcal/mol per HA; compound 6, K_d of 6.3 μM and LE of 0.71 kcal/mol per HA), indicating that the hydroxy modification to compound 6 is not favourable for binding.

Similarly, the hydroxy group of compound 14 is not favourable for binding to hPNMT. In the crystal structure of the hPNMT complex, the hydroxy group is unfavourably close to Met[258] and waters are displaced from the hydrogen-bonding network. These changes result in a reduced enthalpic contribution, a reduced binding affinity and a reduced LE compared with the original hit, compound 6 (compound 14, K_d of 20 μM and LE of 0.58 kcal/mol/HA).

Chloro- and fluoro-substituted 2-aminobenzimidazole compounds (compounds 15 and 16)

Superposition of the fragment hit compounds 6 and 9 bound to hPNMT indicated that a hydrophobic group at the 5-position of the benzimidazole system of compound 6 might contribute additional favourable interactions. To investigate this further, two more compounds were designed: compound 15, combining the 2-amino substituent of compound 6 and the 5-chloro substituent of compound 9; and compound 16 combining the 2-amino substituent of compound 6 and the smaller fluoro substituent at the 5-position (Figure 5). Both compounds 15 and 16 bound as predicted and the 2-chloro derivative compound 15 demonstrated the most favourable binding affinity (K_d of 1.8 μM and LE 0.72 kcal/mol per HA) of this series. The binding affinity of the fluoro-substituted compound 16 (K_d of 7.2 μM), was similar to the parent compound 6, although the enthalpic and entropic contributions were slightly altered, with a less favourable enthalpy but more favourable entropy.

Hydroxy- and chloro-di-substituted 2-aminobenzimidazole (compound 17)

Di-substitution of the 2-aminobenzimidazole core with the 5-chloro and 7-hydroxy substituents in compound 17, did not significantly improve affinity (K_d of 14 μM) compared with the hydroxy substitution alone (compound 13, K_d of 15 μM). As a result, the LE was reduced compared with the original, unsubstituted fragment compound 6, and the separately substituted compounds 13 and 15. Despite extensive trials we were unable to measure X-ray diffraction data for hPNMT–AdoHcy–compound 17. Crystals soaked in this compound cracked during cryoprotection or gave very weak diffraction, indicating that binding of the compound induces crystal disorder or conformational changes to accommodate compound 17. As no improvement in binding affinity or enthalpic contribution was observed, we did not investigate compound 17 further.

DISCUSSION

Using FBS-X we found that 12 compounds from a library of 374 compounds bound to the noradrenaline-binding site of hPNMT by displacing phosphate from the crystal structure. Our hit rate of 3.2 % is similar to that of other FBS-X campaigns [33–38], despite the fact that our target crystal structure was not in the apo form. We also investigated the use of high-sensitivity ESI-FTMS, which has been used previously to screen natural product and combinatorial chemistry libraries against other enzymes [39,40]. For our proof-of-concept study, we used a subset of the fragment library. ESI-FTMS identified the same four hits found by FBS-X for this subset. FBS-MS data acquisition took only 4 min, so an

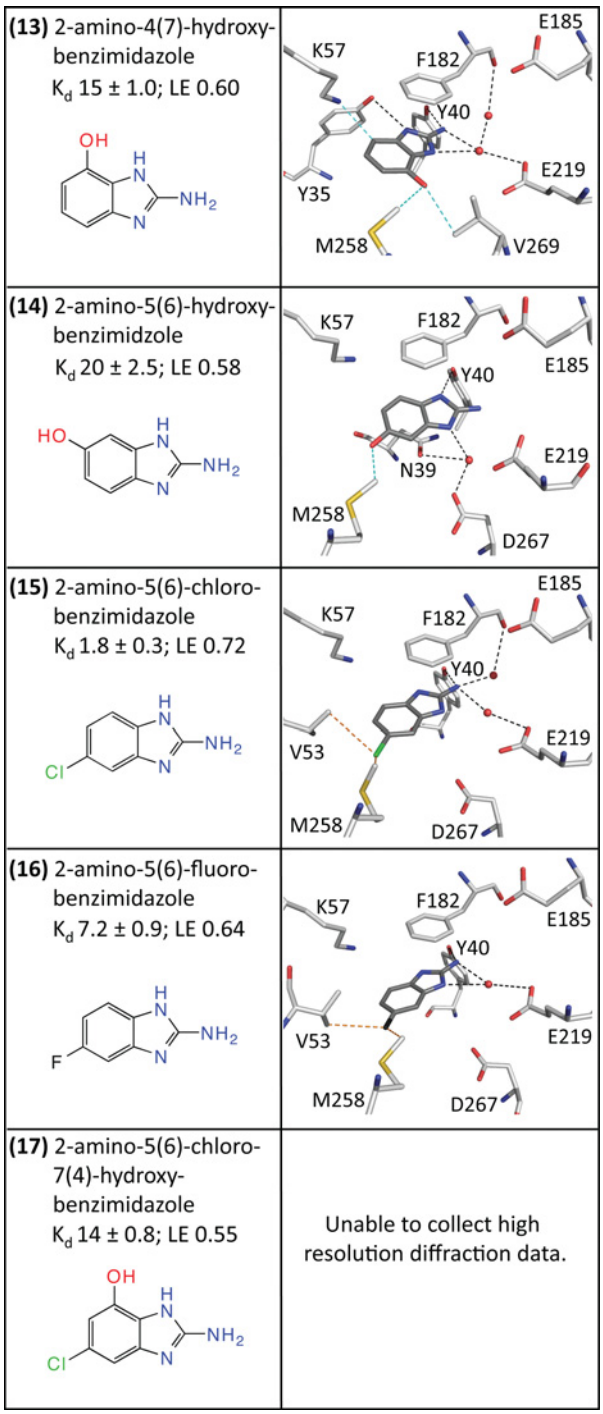

Figure 5 Enzyme–ligand structures and binding information of elaborated benzimidazoles

Chemical structures and binding poses for the elaborated benzimidazole compounds are given (the binding pose for compound 17 is not provided because crystallographic data could not be measured for that complex with hPNMT). Hydrogen bonding interactions are shown in black, hydrophobic interactions in orange and unfavourable interactions in cyan broken lines. Binding affinities determined by ITC (K_d in μM $\pm$ S.D.) and calculated LE values (in kcal/mol per HA) are also indicated.

automated approach could process a 384 compound library in just over 24 h using 0.4 mg of protein. By comparison, our successful FBS-X campaign took 2–3 months and used ~20 mg of protein. These results suggest that ESI-FTMS could be used as a filter to generate a short-list for subsequent characterization by X-ray crystallography. This could in theory reduce the number of crystal structures to be measured from ~150 to ~20, thereby saving time, human resources and protein, and making the technique accessible to many more academic laboratories.

Using ITC we determined the dissociation constants of nine of the 12 FBS-X fragment hits. The results showed that the fragments bind with affinities in the high to low micromolar range and all nine hits for which affinity data were measured had LE values $\geqslant$ 0.4 kcal/mol per HA. Generally, LE values above 0.4 kcal/mol per HA are desirable through the process of optimization [38,41]. Many of our hits had considerably higher LE values, emphasizing their high quality.

Several of the FBS-X hits are benzimidazoles, a known class of PNMT inhibitor. In 1970, researchers at the MSD (Merck Sharp and Dohme Research Laboratories) showed that benzimidazoles (including 2-aminobenzimidazole, compound 6, and 5-chlorobenzimidazole, compound 9) inhibit bovine PNMT. Thus at 28 μg/ml compound 6 inhibits binding of 0.57 mM DL-normetanephrine to bovine PNMT by 30 % and compound 9 inhibits binding by 57 % [32]. Our FBS-X results identified that these compounds also interact with human PNMT and show for the first time how they bind in the noradrenaline pocket. The MSD study also showed that unsubstituted benzimidazole is an inhibitor of bovine PNMT (28 % inhibition under the conditions described above) [32]. Benzimidazole is one of the 376 compounds in the library used in the present study, but was not identified as a hit by FBS-X. This finding could be explained by one or more of the following: (i) benzimidazole does not inhibit PNMT by binding the noradrenaline-binding site; (ii) the noradrenaline-binding site of the human and bovine enzymes differ sufficiently that they recognize benzimidazole differently; or (iii) the screening method we employed is less sensitive than the assay used to detect inhibition in the bovine enzyme.

Several PNMT inhibitors have been shown to be competitive for noradrenaline binding [42–44], although it has been shown that a dichloro-substituted benzimidazole PNMT inhibitor was non-competitive with noradrenaline and uncompetitive with AdoMet [45]. These early results indicate the possibility of an additional binding site for benzimidazoles. Our data clearly show that the three benzimidazole hits and the elaborated compounds bind at the noradrenaline site. However, the hPNMT crystals used for our studies have AdoHcy (as a cofactor product) bound at the AdoMet site. Furthermore, ITC analysis was performed in the presence of excess AdoHcy. Consequently, if the benzimidazole compounds bind to the hPNMT AdoMet site this would not be identified under the conditions of our experiments.

The improved binding affinity of the designed benzimidazole compound 15 compared with the original compound 6, is largely due to an increased entropic contribution to binding (Table 2). Enthalpic optimization is more desirable than entropic opimization in progressing from hit to lead [46]. Typically, enthalpically optimized leads more closely mimic the thermodynamic characteristics of natural protein–ligand interactions, are more soluble and often represent best-in-class compounds in drug discovery programmes [46,47]. Our results therefore indicate that although compound 15 shows higher affinity than compound 6 this improvement may not necessarily correlate with an improved drug lead.

In summary, we have shown that FBS-X can be implemented successfully within an academic environment on a non-ideal protein target. Using FBS-X we identified 12 hits that bind hPNMT at the noradrenaline site. Our pilot study suggests the screening process could be streamlined further by performing FBS-MS first. Three of the FBS-X hits are from a chemical class of known PNMT inhibitors that provide an unanticipated

internal control for the screen. Overall, we structurally and thermodynamically characterized the binding of 17 small molecules to hPNMT, including the first such characterization of the benzimidazole class of compounds bound to the noradrenaline-binding site.

AUTHOR CONTRIBUTION

Nyssa Drinkwater and Jennifer Martin conceived the idea. Nyssa Drinkwater performed the majority of the research and Jennifer Martin co-ordinated the study. Hoan Vu and Sally-Ann Poulsen designed and performed the MS experiments. Kimberly Lovell, Thomas Prisinzano, Kevin Criscione and Gary Grunewald designed and supervized compound synthesis and contributed to compound characterization. Michael McLeish provided the plasmid for the enzyme and contributed to data interpretation. Brett Collins assisted in measurement and analysis of ITC data. Nyssa Drinkwater prepared the first draft of the paper. All authors contributed to discussions on the study and provided intellectual input to the manuscript.

ACKNOWLEDGEMENTS

We are grateful for access to the UQ ROCX Diffraction Facility and thank Karl Byriel and Gordon King for their assistance. We thank staff at the MX1 beamline of the Australian Synchrotron for their invaluable advice. The MS data could not have been measured without access to the Eskitis Institute FTMS facility. We thank Dr F. Anthony Romero for helpful preliminary discussions and Duncan McRee for advice and information regarding the ActiveSight library.

FUNDING

This work was supported by an University of Queensland Graduate School Research Travel Grant and an Australian Postgraduate Award (to N.D.); an Australian Research Council Discovery Project award [grant number DP0664564 (to J.L.M.)]; an Australian National Health and Medical Research Council Biomedical RD Wright Career Development Award (to B.M.C.) and Senior Research Fellowship [grant number 455829 (to J.L.M.)]; an Australian Research Council Linkage Equipment and Infrastructure Award [grant numbers LE0668382 (to J.L.M.), LE237908 (to S.-A.P.)]; and by the National Institutes of Health [grant number NIH HL034193 (to G.L.G.)].

REFERENCES

1 Hajduk, P. J. and Greer, J. (2007) A decade of fragment-based drug design: strategic advances and lessons learned. Nat. Rev. Drug Discov. **6**, 211–219
2 Murray, C. W. and Rees, D. C. (2009) The rise of fragment-based drug discovery. Nat. Chem. **1**, 187–192
3 Congreve, M., Carr, R., Murray, C. and Jhoti, H. (2003) A rule of three for fragment-based lead discovery? Drug Discov. Today **8**, 876–877
4 Rees, D. C., Congreve, M., Murray, C. W. and Carr, R. (2004) Fragment-based lead discovery. Nat. Rev. Drug Discov. **3**, 660–672
5 Erlanson, D. A. (2006) Fragment-based lead discovery: a chemical update. Curr. Opin. Biotech. **17**, 643–652
6 Neumann, T., Junker, H. D., Schmidt, K. and Sekul, R. (2007) SPR-based fragment screening: advantages and applications. Curr. Top. Med. Chem. **7**, 1630–1642
7 Ciulli, A., Williams, G., Smith, A. G., Blundell, T. L. and Abell, C. (2006) Probing hot spots at protein-ligand-binding sites: a fragment-based approach using biophysical methods. J. Med. Chem. **49**, 4992–5000
8 Orita, M., Warizaya, M., Amano, Y., Ohno, K. and Niimi, T. (2009) Advances in fragment-based drug discovery platforms. Exp. Opin. Drug Discov. **4**, 1125–1144
9 Hofstadler, S. A. and Sannes-Lowery, K. A. (2006) Applications of ESI-MS in drug discovery: interrogation of noncovalent complexes. Nat. Rev. Drug Discov. **5**, 585–595
10 Schulz, M. N. and Hubbard, R. E. (2009) Recent progress in fragment-based lead discovery. Curr. Opin. Pharmacol. **9**, 615–621
11 Fuller, R. W. (1982) Pharmacology of brain epinephrine neurons. Ann. Rev. Pharmacol. Toxicol. **22**, 31–55
12 Crowley, W. R., Terry, L. C. and Johnson, M. D. (1982) Evidence for the involvement of central epinephrine systems in the regulation of luteinizing-hormone, prolactin, and growth-hormone release in female rats. Endocrinology **110**, 1102–1107
13 Mefford, I. N., Lister, R. G., Ota, M. and Linnoila, M. (1990) Antagonism of ethanol intoxication in rats by inhibitors of phenylethanolamine N-methyltransferase. Alcohol Clin. Exper. Res. **14**, 53–57
14 Gearhart, D. A., Neafsey, E. J. and Collins, M. A. (2002) Phenylethanolamine N-methyltransferase has β-carboline 2N-methyltransferase activity: hypothetical relevance to Parkinson's disease. Neurochem. Int. **40**, 611–620
15 Kennedy, B. P., Bottiglieri, T., Arning, E., Ziegler, M. G., Hansen, L. A. and Masliah, E. (2004) Elevated *S*-adenosylhomocysteine in Alzheimer brain: influence on methyltransferases and cognitive function. J. Neural Transm. **111**, 547–567
16 Martin, J. L., Begun, J., McLeish, M. J., Caine, J. M. and Grunewald, G. L. (2001) Getting the adrenaline going: crystal structure of the adrenaline-synthesizing enzyme PNMT. Structure **9**, 977–985
17 Drinkwater, N., Gee, C. L., Puri, M., Criscione, K. R., McLeish, M. J., Grunewald, G. L. and Martin, J. L. (2009) Molecular recognition of physiological substrate noradrenaline by the adrenaline-synthesizing enzyme PNMT and factors influencing its methyltransferase activity. Biochem. J. **422**, 463–471
18 Gee, C. L., Tyndall, J. D., Grunewald, G. L., Wu, Q., McLeish, M. J. and Martin, J. L. (2005) Mode of binding of methyl acceptor substrates to the adrenaline-synthesizing enzyme phenylethanolamine N-methyltransferase: implications for catalysis. Biochemistry **44**, 16875–16885
19 McPhillips, T. M., McPhillips, S. E., Chiu, H. J., Cohen, A. E., Deacon, A. M., Ellis, P. J., Garman, E., Gonzalez, A., Sauter, N. K., Phizackerley, R. P. et al. (2002) Blu-Ice and the distributed control system: software for data acquisition and instrument control at macromolecular crystallography beamlines. J. Synchrotron Radiat. **9**, 401–406
20 Otwinowski, Z. and Minor, W. (1997) Processing of X-ray diffraction data collected in oscillation mode. Methods Enzymol. **276**, p.307–326
21 Emsley, P. and Cowtan, K. (2004) COOT: model-building tools for molecular graphics. Acta Crystallogr. Sect. D Biol. Crystallogr. **60**, 2126–2132
22 Schuettelkopf, A. W. and van Aalten, D. M. F. (2004) PRODRG – a tool for high-throughput crystallography of protein–ligand complexes. Acta Crystallogr. Sect. D Biol. Crystallogr. **60**, 1355–1363
23 Adams, P. D., Afonine, P. V., Bunkoczi, G., Chen, V. B., Davis, I. W., Echols, N., Headd, J. J., Hung, L. W., Kapral, G. J., Grosse-Kunstleve, R. W. et al. (2010) PHENIX: a comprehensive Python-based system for macromolecular structure solution. Acta Crystallogr. Sect. D Biol. Crystallogr. **66**, 213–221
24 Grunewald, G. L., Romero, F. A., Chieu, A. D., Fincham, K. J., Bhat, S. R. and Criscione, K. R. (2005) Exploring the active site of phenylethanolamine N-methyltransferase: 3-alkyl-7-substituted-1,2,3,4-tetrahydroisoquinoline inhibitors. Bioorg. Med. Chem. **13**, 1261–1273
25 Morningstar, M. L., Roth, T., Farnsworth, D. W., Smith, M. K., Watson, K., Buckheit, R. W., Das, K., Zhang, W. Y., Arnold, E., Julias, J. G. et al. (2007) Synthesis, biological activity, and crystal structure of potent nonnucleoside inhibitors of HIV-1 reverse transcriptase that retain activity against mutant forms of the enzyme. J. Med. Chem. **50**, 4003–4015
26 Galan, A. A., Chen, J., Du, H., Forsyth, T., Huynh, T. P., Johnson, H. W. B., Kearney, P., Leahy, J. W., Lee, M. S., Mann, G. et al. (2008) Preparation of 1*H*-imidazole-4,5-dicarboxamides as JAK-2 modulators. European Patent Foundation no. WO2008042282-A2
27 Parmee, E. R., Kim, R. M., Rouse, E. A., Schmidt, D. R., Sinz, C. J. and Chang, J. (2005) Preparation of cyclic guanidines as glucagon receptor antagonists for the treatment of type 2 diabetes. PCT Int. Appl., no. WO 2005065680-A1 20050721
28 Gee, C. L., Drinkwater, N., Tyndall, J. D. A., Grunewald, G. L., Wu, Q., McLeish, M. J. and Martin, J. L. (2007) Enzyme adaptation to inhibitor binding: a cryptic binding site in phenylethanolamine N-methyltransferase. J. Med. Chem. **50**, 4845–4853
29 McMillan, F. M., Archbold, J., McLeish, M. J., Caine, J. M., Criscione, K. R., Grunewald, G. L. and Martin, J. L. (2004) Molecular recognition of sub-micromolar inhibitors by the epinephrine-synthesizing enzyme phenylethanolamine N-methyltransferase. J. Med. Chem. **47**, 37–44
30 Wu, Q., Gee, C. L., Lin, F., Tyndall, J. D., Martin, J. L., Grunewald, G. L. and McLeish, M. J. (2005) Structural, mutagenic, and kinetic analysis of the binding of substrates and inhibitors of human phenylethanolamine N-methyltransferase. J. Med. Chem. **48**, 7243–7252
31 Turnbull, W. B. and Daranas, A. H. (2003) On the value of c: can low affinity systems be studied by isothermal titration calorimetry? J. Am. Chem. Soc. **125**, 14859–14866
32 Mandel, L. R., Porter, C. C., Kuehl, F. A., Jensen, N. P., Schmitt, S. M., Windholz, T. B., Beattie, T. R., Carty, J. A., Christen, B. G. and Shen, T. Y. (1970) Inhibition of adrenal phenethanolamine N-methyltransferase by substituted benzimidazoles. J. Med. Chem. **13**, 1043–1047
33 Antonysamy, S. S., Aubol, B., Blaney, J., Browner, M. F., Giannetti, A. M., Harris, S. F., Hebert, N., Hendle, J., Hopkins, S., Jefferson, E. et al. (2008) Fragment-based discovery of hepatitis C virus NS5b RNA polymerase inhibitors. Bioorg. Med. Chem. Lett. **18**, 2990–2995
34 Bosch, J., Robien, M. A., Mehlin, C., Boni, E., Riechers, A., Buckner, F. S., Van Voorhis, W. C., Myler, P. J., Worthey, E. A., DeTitta, G. et al. (2006) Using fragment cocktail crystallography to assist inhibitor design of *Trypanosoma brucei* nucleoside 2-deoxyribosyltransferase. J. Med. Chem. **49**, 5939–5946

35 Lesuisse, D., Lange, G., Deprez, P., Benard, D., Schoot, B., Delettre, G., Marquette, J. P., Broto, P., Jean-Baptiste, V., Bichet, P. et al. (2002) SAR and X-ray. A new approach combining fragment-based screening and rational drug design: application to the discovery of nanomolar inhibitors of Src SH2. J. Med. Chem. **45**, 2379–2387
36 Nienaber, V. L., Richardson, P. L., Klighofer, V., Bouska, J. J., Giranda, V. L. and Greer, J. (2000) Discovering novel ligands for macromolecules using X-ray crystallographic screening. Nat. Biotech. **18**, 1105–1108
37 Schuffenhauer, A., Ruedisser, S., Marzinzik, A. L., Jahnke, W., Blommers, M., Selzer, P. and Jacoby, E. (2005) Library design for fragment based screening. Curr. Top. Med. Chem. **5**, 751–762
38 Wyatt, P. G., Woodhead, A. J., Berdini, V., Boulstridge, J. A., Carr, M. G., Cross, D. M., Davis, D. J., Devine, L. A., Early, T. R., Feltell, R. E. et al. (2008) Identification of N-(4-piperidinyl)-4-(2,6-dichlorobenzoylamino)-1H-pyrazole-3-carboxamide (AT7519), a novel cyclin dependent kinase inhibitor using fragment-based X-ray crystallography and structure based drug design. J. Med. Chem. **51**, 4986–4999
39 Poulsen, S. A. (2006) Direct screening of a dynamic combinatorial library using mass spectrometry. J. Am. Soc. Mass Spec. **17**, 1074–1080
40 Vu, H., Pharm, N. B. and Quinn, R. J. (2008) Direct screening of natural product extracts using mass spectrometry. J. Biomol. Screen. **13**, 265–275

Received 27 April 2010/29 June 2010; accepted 20 July 2010
Published as BJ Immediate Publication 20 July 2010, doi:10.1042/BJ20100651

41 Bembenek, S. D., Tounge, B. A. and Reynolds, C. H. (2009) Ligand efficiency and fragment-based drug discovery. Drug Discov. Today **14**, 278–283
42 Fuller, R. W., Hemrick-Luecke, S. K. and Perry, K. W. (1983) Inhibition of brain epinephrine synthesis by 3,4-dichlorophenylethanolamine, a competitive substrate for norepinephrine N-methyltransferase. Biochem. Pharmacol. **32**, 215–220
43 Fuller, R. W., Roush, B. W., Snoddy, H. D., Day, W. A. and Molloy, B. B. (1975) Norepinephrine N-methyltransferase inhibition by benzamidines, phenylacetamidines, benzylguanidines, and phenylethylguanidines. J. Med. Chem. **18**, 304–307
44 Fuller, R. W., Roush, B. W., Snoddy, H. D. and Molloy, B. B. (1973) Inhibition of phenylethanolamine N-methyltransferase by benzylamines. 2. *In-vivo* studies with 2,3-dichloro-α-methylbenzylamine. J. Med. Chem. **16**, 106–109
45 Pendleton, R. G., Green, H., Snow, I. B., Wang, J. and Kaiser, C. (1972) Studies on the mechanism of phenylethanolamine-N-methyl-transferase inhibition by a dichloro-substituted benzimidazole. Biochem. Pharmacol. **21**, 2967–2975
46 Ladbury, J. E., Klebe, G. and Freire, E. (2010) Adding calorimetric data to decision making in lead discovery: a hot tip. Nat. Rev. Drug Discov. **9**, 23–27
47 Freire, E. (2008) Do enthalpy and entropy distinguish first in class from best in class? Drug Discov. Today **13**, 869–874

Biochem. J. (2010) **431**, 51–61 (Printed in Great Britain) doi:10.1042/BJ20100651

online data

SUPPLEMENTARY ONLINE DATA

Fragment-based screening by X-ray crystallography, MS and isothermal titration calorimetry to identify PNMT (phenylethanolamine N-methyltransferase) inhibitors

Nyssa DRINKWATER*, Hoan VU†, Kimberly M. LOVELL‡, Kevin R. CRISCIONE‡, Brett M. COLLINS*, Thomas E. PRISINZANO‡, Sally-Ann POULSEN†, Michael J. McLEISH§, Gary L. GRUNEWALD‡ and Jennifer L. MARTIN*[1]

*University of Queensland, Institute for Molecular Bioscience, Division of Chemistry and Structural Biology, Brisbane, Queensland 4072, Australia, †Griffith University, Eskitis Institute, Brisbane, Queensland 4111, Australia, ‡Department of Medicinal Chemistry, University of Kansas, Lawrence, KS 66045-7582, U.S.A., and §Department of Chemistry and Chemical Biology, Indiana University–Purdue University Indianapolis (IUPUI), 402 N. Blackford St, LD 326D, IN 46202, U.S.A.

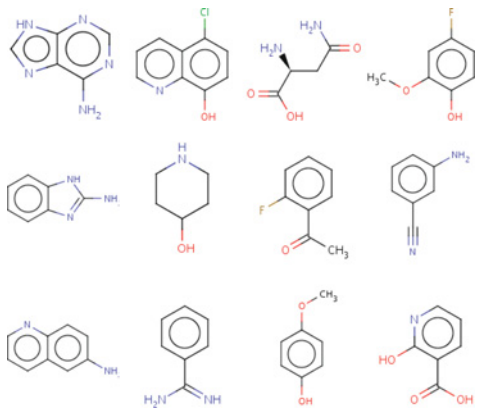

Figure S1 Chemical structures of fragments screened by MS

EXPERIMENTAL

Chemical synthesis details for compounds 14, 15 and 16

2-Amino-5(6)-hydroxybenzimidazole hydrobromide (compound 14 · HBr)

Benzimidazole compound 14 · HBr was synthesized from 4-methoxybenzene-1,2-diamine in two steps [1,2] (93 % overall yield), m.p. 207–212 °C: ^{1}H-NMR (500 MHz, MeOD) δ 7.16 (t, $J = 7.3$, 1H), 6.78 (d, $J = 2.3$, 1H), 6.72 (dd, $= 2.3$, 8.6, 1H); ^{13}C-NMR (126 MHz, MeOD) δ 156.1, 152.1, 132.0, 124.0, 113.0, 112.7, 99.3; HRMS (*m*/*z*): [M+H] calculated for $C_7H_7N_3OBr$, 227.9772; found 227.9783.

2-Amino-5(6)-chlorobenzimidazole hydrobromide (compound 15 · HBr)

Benzimidazole (compound 15 · HBr) was synthesized according to the procedure described previously [3] from 4-chlorobenzene-1,2-diamine (0.50 g, 3.5 mmol). After stirring overnight, the cyanogen bromide reaction mixture was evaporated under reduced pressure to give compound 15 · HBr as a brown solid, which was recrystallized from 2-propanol/hexanes (0.39 g, 46 %), m.p. 241–243 °C: ^{1}H-NMR (500 MHz, MeOD) δ 7.39 (d, $J = 1.9$, 1H), 7.34 (d, $J = 8.5$, 1H), 7.27 (dd, $J = 1.9$, 8.5, 1H); ^{13}C-NMR (126 MHz, MeOD) δ 153.0, 132.1, 130.3, 130.0, 125.1, 113.6, 112.7; HRMS (*m*/*z*): [M+H] calculated for $C_7H_7N_3Cl$, 168.0329; found 168.0332.

A sample of (compound 15 · HBr) was dissolved in aqueous NaOH (1.25 M, 20 ml) and extracted with diethyl ether (3× 15 ml). The combined organic layers were washed with brine (10 ml) and dried over Na_2SO_4. The solvent was evaporated under reduced pressure and the resulting residue was triturated with hexanes/ethyl acetate (3:1) to afford compound 15 as a yellow solid: m.p. 165–170 °C (compared with the reported m.p. of 167–168 °C [3]).

2-Amino-5(6)-fluorobenzimidazole hydrobromide (compound 16 · HBr)

Benzimidazole compound 16 · HBr was synthesized according to the procedure described previously [4] in two steps from 4-fluoro-2-nitroaniline (1.1 g, 7.0 mmol) with the following modifications: (i) the reduction step was carried out at atmospheric pressure; and (ii) after stirring overnight, the cyanogen bromide reaction mixture was evaporated under reduced pressure to give a brown oil. Trituration with 2-propanol/diethyl ether yielded compound 16 · HBr as a viscous brown liquid that was dried *in vacuo* to a brown solid (0.11 g, 6.6 % overall yield), m.p. 212–220 °C; ^{1}H-NMR (500 MHz, MeOD) δ 7.36 (dd, $J = 4.3$, 8.8, 1H), 7.16 (dd, $J = 2.4$, 8.4, 1H), 7.04 (ddd, $J = 2.5$, 8.8, 9.7, 1H); ^{13}C-NMR (126 MHz, MeOD) δ 161.2 (d, $J = 239.4$), 153.2 (s), 131.8 (d, $J = 12.6$), 127.5 (s), 113.4 (d, $J = 10.1$), 112.0 (d, $J = 25.2$), 100.3 (d, $J = 30.2$); HRMS (*m*/*z*): [M+H] calculated for $C_7H_7N_3F$, 152.0624; found 152.0627.

[1] To whom correspondence should be addressed (email j.martin@imb.uq.edu.au).

The co-ordinates and structure factors for all 17 crystal structures have been deposited with the PDB under codes 3KPJ, 3KPU, 3KPV, 3KPW, 3KPY, 3KQM, 3KQS, 3KQT, 3KQV, 3KQW, 3KQO, 3KQP, 3KQQ, 3KQY, 3KR0, 3KR1 and 3KR2.

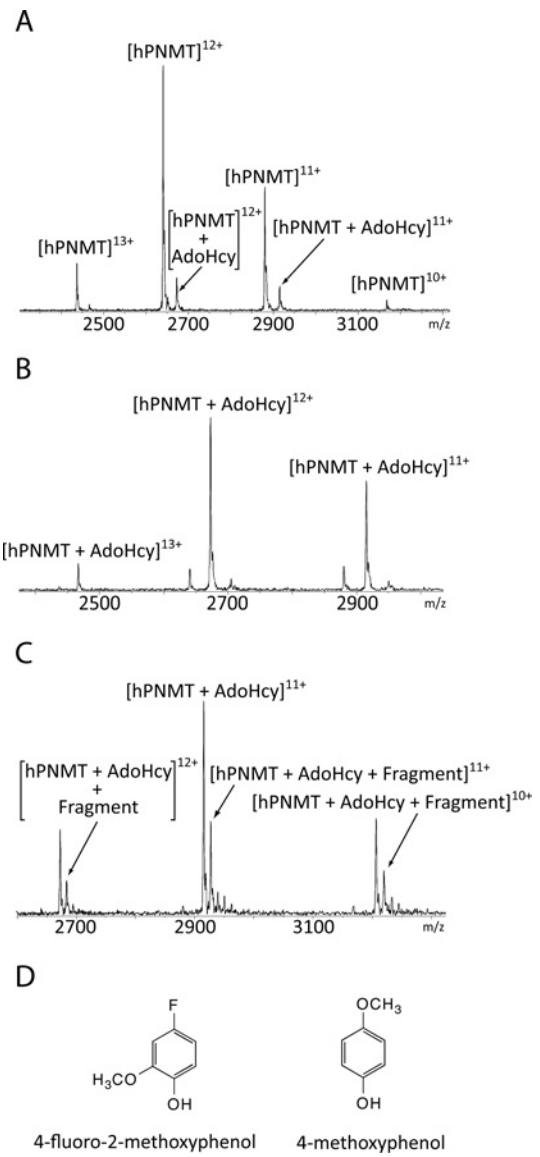

Figure S2 ESI-FTMS screening

(**A)** ESI-FTMS positive ion mass spectrum of hPNMT (3 μM) in 10 mM ammonium acetate solution. Peaks corresponding to hPNMT in complex with AdoHcy are also observed indicating a small amount of AdoHcy co-purifies with the enzyme. (**B**) ESI-FTMS positive ion mass spectrum of a mixture of hPNMT (3 μM) and AdoHcy (30 μM) in 10 mM ammonium acetate and 5 % methanol. (**C**) ESI-FTMS positive ion mass spectrum of a mixture of hPNMT (3 μM), AdoHcy (30 μM) and compound 6 (300 μM) in 10 mM ammonium acetate and 5 % methanol. (**D**) Structures of the two additional fragments detected by ESI-FTMS, but not detected by FBS-X or ITC.

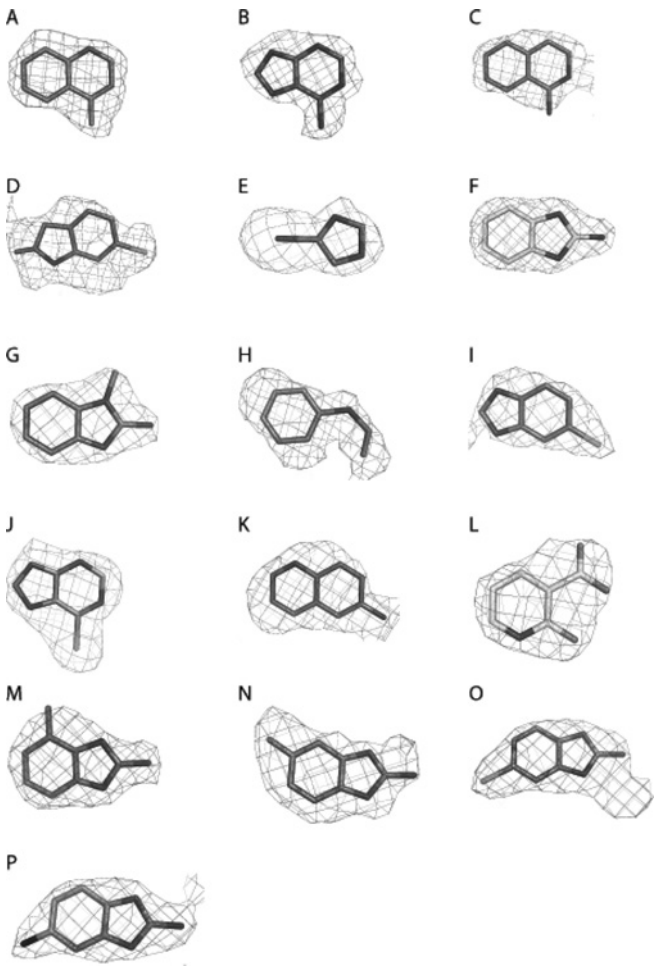

Figure S3 Electron density ($2F_o-F_c$ shown at 1σ) for ligands bound to hPNMT

(**A**–**P**) represent density for compounds 1–17.

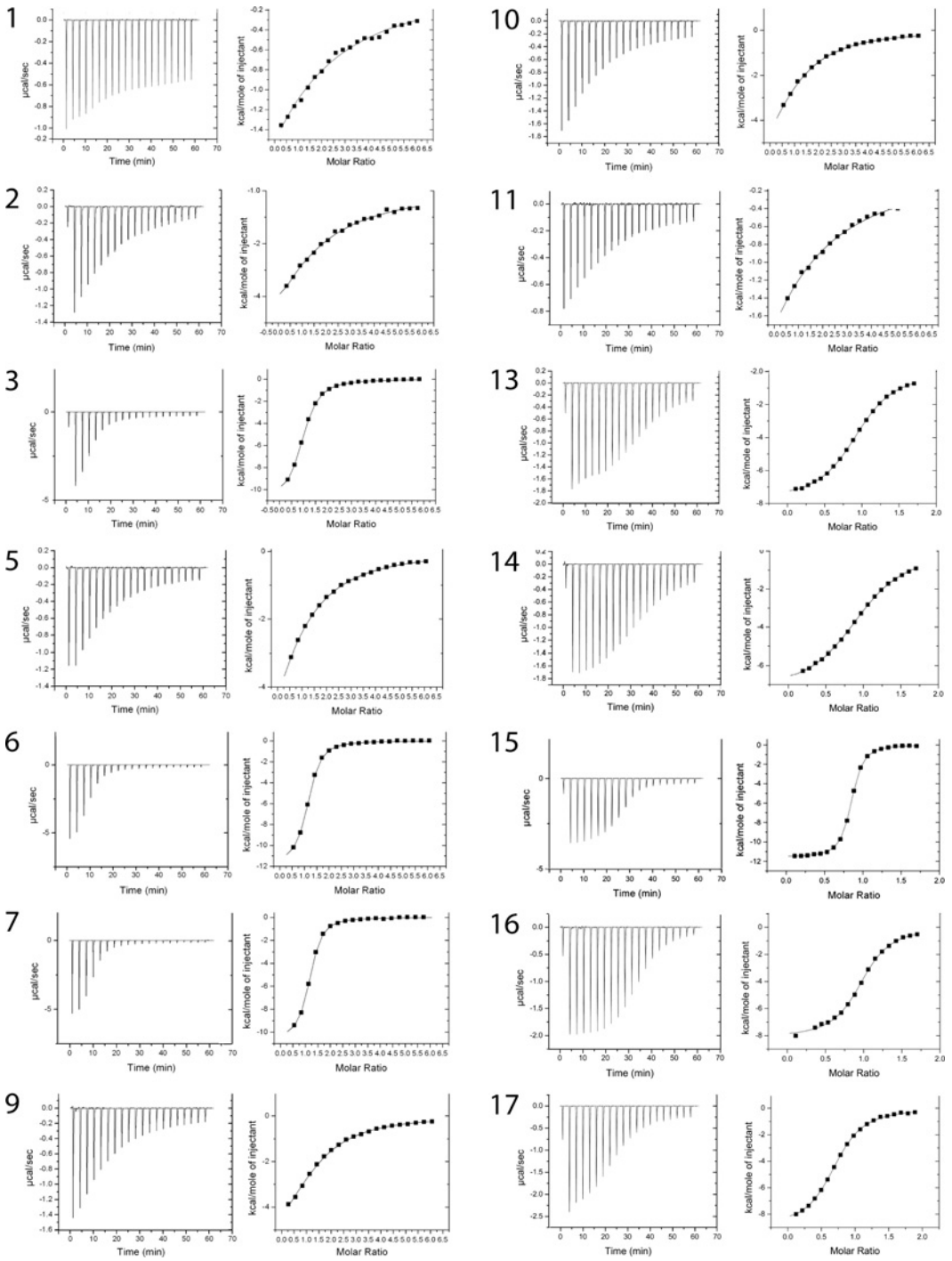

Figure S4 ITC curves for fragment hits and derivatized benzimidazoles binding to hPNMT

Table S1 Mass/charge (*m/z*) values for hPNMT and hPNMT bound ligands (AdoHcy and compound 6) identified from screening of compound 6 by MS

The molecular mass of the fragment of compound 6 is calculated according to: M_r fragment $= D m/z \times z = [m/z$ (hPNMT–AdoHcy–fragment)$- m/z$ (hPNMT–AdoHcy)$] \times z$

Charge state (z)	m/z (hPNMT)	m/z (hPNMT–AdoHcy)	m/z (hPNMT–AdoHcy–fragment)	M_r fragment
13^+	2437.6	2467.1	–	–
12^+	2641.0	2673.1	2684.0	130.8
11^+	2880.6	2915.6	2927.6	132.0
10^+	3168.2	3206.9	3220.1	132.0

Table S2 Crystallographic data and refinement statistics for structures of fragment hits in complex with hPNMT–AdoHcy

The data for fragment hit compounds 1–5 were collected in house using the UQ ROCX Diffraction Facility, whereas the data for fragment hit compounds 6–12 were collected at the Australian Synchrotron (3BM1). The completeness is number of measured unique reflections divided by the number of theoretical reflections, expressed as a percentage. $R_{merge} = \Sigma|I_{obs} - I_{av}|/\Sigma I_{av}$, over all symmetry-related observations. $R_{cryst} = \Sigma|F_{obs} - F_{calc}|/\Sigma|F_{obs}|$, over all reflections. R_{free} is calculated as for R_{cryst} from 5–10 % of the data excluded from refinement. Values in parentheses are for the highest resolution shell of data.

	Fragment hit												
Parameter	–	1	2	3	4	5	6	7	8	9	10	11	12
Space group	$P4_32_12$	$P4_32_12$	$P4_32_12$	$P4_32_12$	$P4_32_12$	$P4_32_12$	$P4_32_12$	$P4_32_12$	$P4_32_12$	$P4_32_12$	$P4_32_12$	$P4_32_12$	$P4_32_12$
Unit cell													
a,b (Å)	94.4	94.4	94.2	94.3	93.9	93.8	94.7	93.9	94.4	94.4	94.3	93.6	94.0
c (Å)	186.9	188.5	188.8	188.6	188.6	188.7	189.2	188.5	189.4	189.5	189.0	188.8	188.9
α,β,γ (°)	90	90	90	90	90	90	90	90	90	90	90	90	90
No. observations	112323	150000	196450	179390	149936	228299	510457	317982	325385	211596	171507	151324	147430
No. unique reflections	29790	31980	28540	33323	30511	30146	58278	33746	38736	28974	33145	30322	26826
Resolution (Å)	33.38–2.50 (2.59– 2.50)	35.03–2.40 (2.49–2.40)	45.69–2.40 (2.49–2.40)	37.73–2.40 (2.49–2.40)	45.56–2.40 (2.49–2.40)	45.63–2.40 (2.49–2.40)	50.00–2.00 (2.01–2.00)	50.00–2.40 (2.49–2.40)	50.00–2.30 (2.38–2.30)	50.0–2.50 (2.59–2.50)	47.13–2.40 (2.49–2.40)	45.41– 2.40 (2.49–2.40)	38.40–2.50 (2.59–2.50)
Redundancy	3.8 (3.8)	4.7 (3.2)	6.9 (7.1)	5.4 (2.6)	4.9 (3.9)	7.6 (6.1)	8.8 (6.3)	9.4 (8.3)	8.4 (7.8)	7.3 (3.5)	5.2 (3.2)	5.0 (3.5)	5.5 (4.8)
$I/\sigma I$	11.7 (2.2)	5.3 (2.2)	10.5 (6.4)	12.1 (1.6)	8.6 (3.8)	6.8 (3.0)	8.7 (1.6)	9.1 (2.7)	12.4 (5.1)	6.5 (0.9)	6.7 (2.1)	6.2 (2.9)	7.3 (2.6)
Completeness (%)	99.1 (99.9)	93.8 (88.3)	83.8 (54.3)	97.7 (90.1)	90.2 (75.0)	89.3 (68.3)	99.6 (98.5)	99.7 (99.8)	99.6 (99.7)	93.6 (62.5)	97.1 (89.3)	90.3 (82.9)	89.2 (82.4)
R_{merge} (%)	5.0 (52.5)	15.1 (43.6)	10.0 (24.6)	7.1 (43.9)	9.6 (27.6)	15.3 (46.2)	7.5 (5.6)	7.7 (54.6)	5.5 (28.1)	14.3 (58.5)	12.3 (43.3)	13.8 (33.8)	11.7 (42.9)
Refinement													
R_{cryst}/R_{free} (%)	21.1/26.7	22.7/29.1	21.4/27.2	21.2/28.4	20.6/27.1	22.7/29.2	18.8/21.7	18.1/23.4	18.4/23.0	19.4/26.2	21.9/27.9	23.1/30.2	22.5/30.6

Table S3 Crystallographic data and refinement statistics for structures of elaborated benzimidazole compounds 13–16 in complex with hPNMT–AdoHcy

The completeness is number of measured unique reflections divided by the number of theoretical reflections, expressed as a percentage. $R_{merge} = \Sigma|I_{obs} - I_{av}|/\Sigma I_{av}$, over all symmetry-related observations. $R_{cryst} = \Sigma|F_{obs} - F_{calc}|/\Sigma|F_{obs}|$, over all reflections. R_{free} is calculated as for R_{cryst} from 5–10% of the data excluded from refinement. Values in parentheses are for the highest resolution shell of data.

	Compound			
Parameter	13	14	15	16
Space Group	$P4_32_12$	$P4_32_12$	$P4_32_12$	$P4_32_12$
Unit Cell				
a,b (Å)	94.5	94.3	94.1	94.4
c (Å)	188.3	188.5	189.4	188.2
α,β,γ (°)	90	90	90	90
No. observations	184367	83731	134165	148978
No. unique reflections	44046	26367	38506	38507
Resolution (Å)	47.26–2.20 (2.28–2.20)	45.73–2.60 (2.69 - 2.60)	42.30–2.30 (2.38–2.30)	45.72–2.30 (2.38–2.30)
Redundancy	4.19 (4.15)	3.18 (3.16)	3.48 (3.50)	3.87 (3.89)
$I/\sigma I$	10.0 (2.1)	9.6 (2.3)	10.8 (2.3)	10.0 (2.3)
Completeness (%)	99.8 (100.0)	97.8 (99.3)	99.8 (99.8)	99.7 (100.0)
R_{merge} (%)	5.6 (50.3)	6.5 (37.6)	5.0 (42.9)	6.0 (47.7)
Refinement				
R_{cryst}/R_{free} (%)	22.8/26.2	21.7/25.7	21.8/24.9	21.2/24.7

REFERENCES

1 Galan, A. A., Chen, J., Du, H., Forsyth, T., Huynh, T. P., Johnson, H. W. B., Kearney, P., Leahy, J. W., Lee, M. S., Mann, G. et al. (2008) Preparation of 1*H*-imidazole-4,5-dicarboxamides as JAK-2 modulators. European Patent Foundation no. WO2008042282-A2

2 Lattanzi, R., Spetea, M., Schullner, F., Rief, S. B., Krassnig, R., Negri, L. and Schmidhammer, H. (2005) Synthesis and biological evaluation of 14-alkoxymorphinans. 22. Influence of the 14-alkoxy group and the substitution in position 5 in 14-alkoxymorphinan-6-ones on *in vitro* and *in vivo* activities. J. Med. Chem. **48**, 3372–3378

3 Leonard, N. J., Curtin, D. Y. and Beck, K. M. (1947) Sulfonate salts of substituted benzimidazoles. J. Am. Chem. Soc. **69**, 2459–2461

4 Mandel, L. R., Porter, C. C., Kuehl, F. A., Jensen, N. P., Schmitt, S. M., Windholz, T. B., Beattie, T. R., Carty, J. A., Christen, B. G. and Shen, T. Y. (1970) Inhibition of adrenal phenethanolamine N-methyltransferase by substituted benzimidazoles. J. Med. Chem. **13**, 1043–1047

Received 27 April 2010/29 June 2010; accepted 20 July 2010
Published as BJ Immediate Publication 20 July 2010, doi:10.1042/BJ20100651